The Company of **Biologists**

RESEARCH ARTICLE

Intrinsic properties of limb bud cells can be differentially reset

Patricia Saiz-Lopez[1], Kavitha Chinnaiya[2], Matthew Towers[2],*,‡ and Maria A. Ros[1],[3],*,‡

ABSTRACT

An intrinsic timing mechanism specifies the positional values of the zeugopod (i.e. radius/ulna) and then autopod (i.e. wrist/digits) segments during limb development. Here, we have addressed whether this timing mechanism ensures that patterning events occur only once by grafting GFP-expressing autopod progenitor cells to the earlier host signalling environment of zeugopod progenitor cells. We show by detecting *Hoxa13* expression that early and late autopod progenitors fated for the wrist and phalanges, respectively, both contribute to the entire host autopod, indicating that the autopod positional value is irreversibly determined. We provide evidence that Hoxa13 provides an autopod-specific positional value that correctly allocates cells into the autopod, most likely through the control of cell-surface properties as shown by cell-cell sorting analyses. However, we demonstrate that only the earlier autopod cells can adopt the host proliferation rate to permit normal morphogenesis. Therefore, our findings reveal that the ability of embryonic cells to differentially reset their intrinsic behaviours confers robustness to limb morphogenesis. We speculate that this plasticity could be maintained beyond embryogenesis in limbs with regenerative capacity.

KEY WORDS: Limb development, Proximo-distal, Hoxa13, Chick, Proliferation

INTRODUCTION

Developmental patterning events occur in a linear sequence over time and are only repeated in tissues in which regeneration is possible, such as the adult limbs of some amphibians. During tetrapod limb development, the three proximo-distal segments are specified in sequence, with the progenitor cells located under the apical ectodermal ridge progressively transiting through specification states corresponding to the stylopod, the zeugopod and then the autopod (Tabin and Wolpert, 2007; Towers et al., 2012; Delgado and Torres, 2016). The mechanisms by which limb progenitor cells acquire progressively more distal fates have been subject to intense investigation over many years (Delgado and Torres, 2016). We recently presented a complete model of embryonic proximo-distal (PD) limb development that is composed of two sequential phases (Saiz-Lopez et al., 2015). During the initial phase, signals from the flank of the embryo and from the distal tip of the emerging limb bud specify the structures of

the stylopod (i.e. humerus/femur) (Cooper et al., 2011; Roselló-Díez et al., 2011). This is followed by a second phase in which an intrinsic timing mechanism progressively specifies the more-distal structures of the zeugopod (i.e. radius/ulna) and then the autopod (i.e. the digits) (Roselló-Díez et al., 2014; Saiz-Lopez et al., 2015). This intrinsic timer operates in distal limb mesenchyme cells after they have been freed from the influence of proximal signals as a consequence of growth of the bud. The timing mechanism involves the progressive transition from a proximal to a distal mode of 5′ Hox gene expression, deceleration of proliferation rate and changes in cell surface adhesion properties, as well as the maintenance of the overlying apical ectodermal ridge (AER), a thickening of the epithelium that rims the distal tip of the limb bud and that is essential for limb bud outgrowth (Fernandez-Teran and Ros, 2008). Maintenance of the AER allows it to produce permissive signals based on fibroblast growth factor (FGF) signalling that sustain the intrinsic timer operating in the underlying mesenchyme for the appropriate duration.

Here, we have investigated when the progressive specification of the autopod fate becomes irreversibly determined and which intrinsically regulated processes prevent patterning events from reoccurring. To address these questions we transplanted labelled cells in different phases of late (old) PD limb specification to an earlier (younger) environment to determine the stability and reversibility of their developmental potential. This is achieved in the chicken by the use of a transgenic flock/line ubiquitously expressing green fluorescent protein (GFP) that permits the accurate tracing of cell fate when grafted into wild-type embryos (McGrew et al., 2004). We have revealed here that the autopod fate, as determined by *Hoxa13* expression, is stable in later cells grafted to an earlier environment fated for the zeugopod. In our assays, early autopod progenitor cells (fated for elements distal to the wrist) and later cells (fated for the phalanges only) produce equivalent fate maps and contribute to the entire autopod. We show that *Hoxa13* expression provides a segment-specific positional value that likely ensures the correct allocation of *Hoxa13*-positive cells into the autopod. This is consistent with a role of Hoxa13 in the control of cell surface properties. We also show that the early environment can reset the proliferation rate of early autopod progenitor cells, but it cannot reset the proliferation rate of later autopod progenitor cells. This loss of proliferative plasticity in late autopod progenitors leads to discontinuities between host and donor cell proliferation rates, and this results in defective morphogenesis. The implications of these findings for normal and regenerative limb morphogenesis are discussed.

RESULTS

Progenitor cells fated to proximal and distal autopod contribute to the entire autopod when transferred to an earlier environment

We have previously shown that the proximo-distal (PD) positional values of the distal limb segments are progressively acquired through an intrinsic timing mechanism (Saiz-Lopez et al., 2015). To

[1]Departamento de Señalización Celular y Molecular, Instituto de Biomedicina y Biotecnología de Cantabria, IBBTEC (CSIC-Universidad de Cantabria), Santander 39011, Spain. [2]Bateson Centre, Department of Biomedical Science, University of Sheffield, Western Bank, Sheffield S10 2TN, UK. [3]Departamento de Anatomía y Biología Celular, Facultad de Medicina, Universidad de Cantabria, Santander 39011, Spain.
*These authors contributed equally to this work

‡Authors for correspondence (m.towers@sheffield.ac.uk; marian.ros@unican.es)

M.T., 0000-0003-2189-4536; M.A.R., 0000-0002-1224-7671

determine if positional values can be reset, we performed heterochronic grafts of autopod progenitor cells from old donor wing buds, either fated for the proximal wrist (HH24; Hamburger and Hamilton, 1951) or for the distal phalanges (HH27), to distal limb buds of earlier hosts fated for the zeugopod. Previously, we traced the fate of these progenitor cells in the distal tip of the limb using the same procedure, but instead between identical host and donor stages (homochronic grafting). Briefly, the procedure consists of grafting 150 μm blocks of distal mesenchyme cells of donor GFP-expressing chick wings denuded of ectoderm under the AER of wild-type host buds. In homochronic grafts, stage HH20 distal cells gave rise to the zeugopod and autopod while HH24 distal cells produce only the entire autopod (Saiz-Lopez et al., 2015; see blue and red asterisks in Fig. 1L). It should be noted that it is not possible to use this procedure to trace the fate of HH27 distal cells because at this stage the AER is regressing and flattening and thus does not permit the stretching required for grafting. However, previous experiments, including AER removal experiments that truncate limb outgrowth, indicate that HH27 distal cells contribute to the phalanges only (Dudley et al., 2002; Pascoal et al., 2007; Summerbell, 1974; Suzuki et al., 2008).

We heterochronically grafted blocks of 150 μm distal progenitors of HH24 (proximal autopod) or HH27 (distal autopod) GFP-expressing embryos under the AER of earlier HH20 (zeugopod progenitors) wild-type host wing buds (Fig. 1A-C,D-F). Analyses of day 11 host embryos showed that the donor HH24 GFP-expressing cells, which are older than the host by 24 h, gave rise to their expected fate map of the whole autopod (n=7/7; Fig. 1B,C and black asterisks in L) and were not reset to the host HH20 fate map of the zeugopod. Surprisingly, HH27 GFP-expressing donor cells, older than the host by 48 h, also gave rise to the whole autopod (n=16/16; Fig. 1E,F and brown asterisks in L), rather than their predicted positional value of the digits only and therefore produced similar fate maps to grafts of HH24 distal limb progenitors. The proximal limit of the grafted tissue at the level of the carpus was confirmed in histological sections hybridized for *Gfp* as shown in Fig. 1J for a HH27-20 graft. The grafted tissue contributed to the phalanges, metacarpals and a carpal, as well as the surrounding soft tissues, as seen in consecutive sections (7 μm apart) hybridized for *Sox9* (Fig. 1K). Thus, when transferred to an earlier environment, distal HH24 and HH27 progenitor cells show a similar contribution to the PD axis, disregarding their distinct presumptive fates. Interestingly, although the grafted cells were initially placed in the host in a position that would normally contribute to the zeugopod, they became entrained into the autopod. A possible interpretation of these results is that the positional value, and thus the morphogenetic potential of all autopod progenitors, is equivalent.

In addition, an unexpected finding was that, while skeletal development appeared normal in HH20 wing buds with HH24 grafts (n=6/7; Fig. 1C,M), it was defective in HH20 wing buds with HH27 grafts (n=15/16; Fig. 1F,M). Although in such wings with grafts, the stylopod and zeugopod segments were correctly proportioned, the autopod was reduced in length by 30% and was often severely twisted (Fig. 1F,M). To determine whether this defect was merely a consequence of the age of the donor tissue (48 h older than the host), or in contrast, was due to the particular development stage (HH27) of the graft (fated for the phalanges), we performed two serial grafts of HH24 GFP-expressing distal progenitors to HH20 host wing buds (Fig. 1G). In such serial experiments, 24 h after the first graft, a distal block (150 μm) of GFP-expressing cells was again transferred to a new HH20 host wing bud and allowed to develop (see Materials and Methods). Therefore, although the age of the second serial graft was
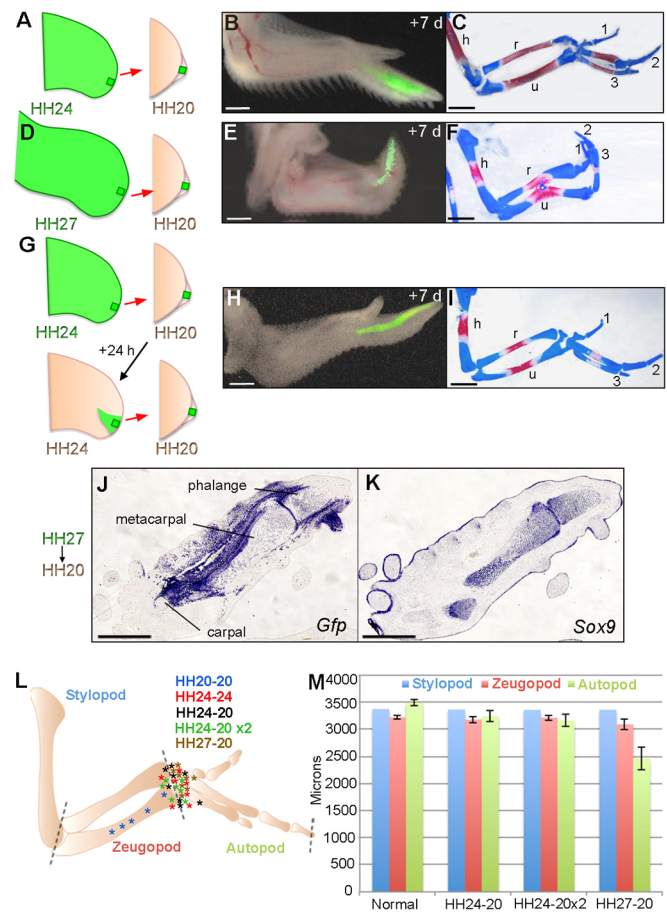
Fig. 1. Proximal and distal autopod progenitors display similar positional values when grafted to a young environment. (A-C) GFP-expressing HH24 distal cells (150 μm blocks) grafted under the AER of earlier wild-type HH20 wings give rise to structures distal to the wrist without perturbing the morphogenesis of the host. (D-F) GFP-expressing HH27 distal cells (150 μm blocks) display similar positional values but the development of the host autopod is disrupted. (G-I) GFP-expressing HH24 distal mesenchyme tissue subject to two consecutive grafts spaced 24 h apart also give rise to structures distal to the wrist without altering the morphogenesis of the host. For each experiment, the schematic is depicted on the left followed by the picture of the 11-day-old specimen under UV light to visualize the graft and the skeletal preparation. (J,K) Consecutive sections of a HH27 graft 7 days after implantation hybridized for *Gfp* and *Sox9* as indicated. Note that the proximal boundary of the grafted tissue lies at the wrist and that the *Gfp*-expressing cells have integrated in all type of tissues. (L) Schematic summary representation of the developmental potential of the grafts. Each asterisk represents the proximal boundary of the grafted tissue for each experiment. The fate of homochronic HH20 to HH20 (blue) and HH24 to HH24 (black) from Saiz-Lopez et al. (2015) is also depicted. (M) Histogram showing the length distribution of the host limb segments in each of the grafting experiments performed. Only the autopod of HH20 host with HH27 grafts shows a statistically significant reduction in length. The GFP-expressing tissue is depicted as green in this and all schematic representations. Data are mean±s.e.m. of n=34 for normal, 8 for HH24-20, 13 for HH24-20x2 and 15 for HH27-20. Scale bars: 1 mm (B-I) and 600 μm (J,K).

the same as a single HH27 graft, it had not been in an environment later than HH24. Analyses of day 11 embryos showed that the serially grafted GFP-expressing HH24 cells contributed to the complete autopod (n=12; Fig. 1G-I and green asterisks in L), and produced similar fate maps to those of both HH24 and HH27 grafts (Fig. 1H,L). However, unlike HH20 wings with HH27 grafts (Fig. 1E,F), HH20 wings with serially grafted HH24 cells appeared morphologically normal at day 11, with correctly proportioned skeletons (Fig. 1I,M). This result shows that it is the developmental

stage, and not the actual age of distal grafts, that perturbs the morphogenesis of the earlier host wing. It also indicates that the young environment of HH20 can prevent HH24 cells from progressing to the stage corresponding to their own age (HH27).

In summary, our analyses show that early and late autopod progenitor cells produce similar fate maps when grafted to early limb buds. However, the behaviour of these two types of grafts is distinct, as only the later grafts fail to integrate/coordinate with host tissues and this disrupts the normal morphology of the host wing.

Stable *Hoxa13* expression in autopod grafts can explain their similar fates

To understand why proximal (HH24) and distal (HH27) autopod progenitors show an equivalent PD potential when placed in an HH20 environment, we analysed the dynamics of expression of *Hoxa13*, the best marker of the autopod (Scotti et al., 2015; Tabin and Wolpert, 2007), in heterochronic grafts. In the chick wing bud, *Hoxa13* expression is initiated at HH22 in an intrinsically timed manner and continues to be expressed through development, at least until day 10 (Saiz-Lopez et al., 2015). In our experiments, either grafts of HH24, HH27, or two serial grafts of HH24 GFP-expressing distal cells maintained expression of *Hoxa13* when grafted under the AER of HH20 host buds (Fig. 2). The expression of *Hoxa13* made the grafts clearly distinguishable as they became progressively embedded in the incipient domain of host *Hoxa13* expression. Importantly, the presence of the graft did not interfere with the normal dynamics of *Hoxa13* activation in the host (Fig. 2A-I). For instance, 24 h after transplantation, the three types of grafts expressed *Hoxa13* and were still surrounded at their proximal levels by non-expressing proximal host tissues (asterisks in Fig. 2G-O). The grafts were clearly visualized by their expression of *Gfp* in adjacent sections (7 μm apart) to those hybridized for *Hoxa13*. Around 48 h after grafting, the grafts had become embedded in the host *Hoxa13* domain as shown for a HH27 graft in Fig. 2P-R). However, it should be noted that, in most instances, even after the graft was completely embedded in the host *Hoxa13* domain, it could still be distinguished as a result of differences in the amount of *Hoxa13* transcripts between host and donor tissue. It remains to be determined whether this observation reflects the possibility that a specific level of *Hoxa13* expression is intrinsically determined throughout development. The fact that the three types of grafts become completely entrained within the evolving host domain of *Hoxa13* expression (see schematics in Fig. 2) suggests that Hoxa13 allocates the grafted cells into the host autopod.

Thus, our results show that *Hoxa13* expression is stable in single and serial grafts of HH24 and of HH27 cells made to earlier buds, and that the distal signalling environment of the early bud does not abolish the expression of *Hoxa13*. It is known that Fgf signalling from the AER is required for *Hoxa13* activation but it cannot induce its expression (Vargesson et al., 2001; Roselló-Díez et al., 2014). To determine whether Fgf signalling is also required, we grafted blocks of HH24 and HH27 GFP-expressing distal progenitors to proximal (stylopod or zeugopod level) of HH20 wild-type host. Our results showed that even 48 h after grafting the expression of *Hoxa13* was clearly detected in the grafts, indicating that AER influence is not required for maintenance of expression (Fig. S1). Therefore, once activated, *Hoxa13* expression seems to be independent of AER signalling.

Cell-cell affinities are segment specific and correlate with *Hoxa13* expression

The observation that grafted autopod progenitor cells are entrained into the prospective autopod instead of contributing to the
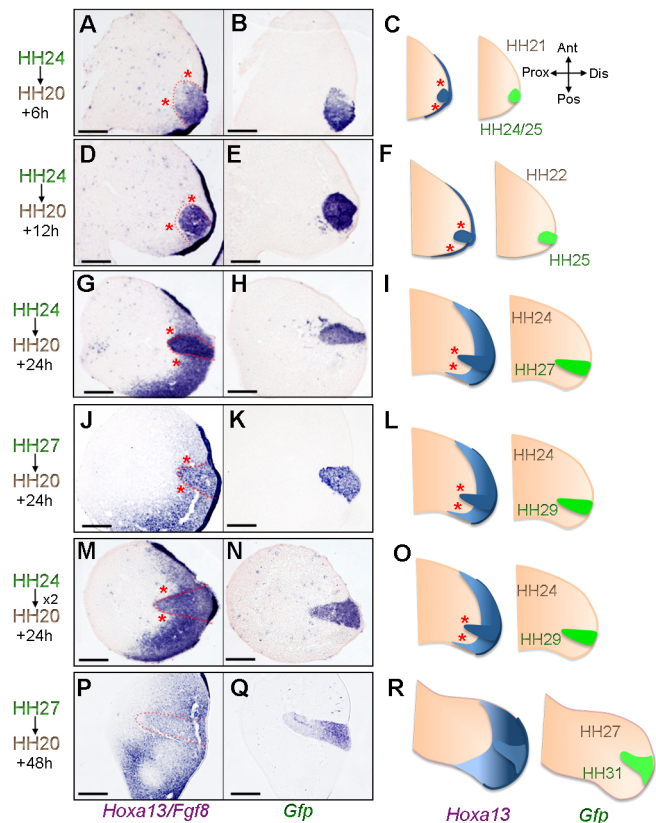
Fig. 2. *Hoxa13* expression is robustly maintained in the grafted tissue. Frontal (flat) sections of host limbs showing stable expression of *Hoxa13* (also hybridized for *Fgf8*) in the graft irrespective of the earlier host environment (A,D,G,J,M,P). The position of the graft is assessed by *in situ* hybridization for *Gfp* in consecutive, 7 μm apart, sections (B,E,H,K,N,Q). The type of graft is indicated on the left and the schematics, including the expression patterns of *Hoxa13* (dark blue) and *Gfp* (bright green) on the left (C,F,I,L,O,R). The age of the host (brown) and grafts (green) at the time of the analysis is also indicated in the schematics. Note that 24 h after implantation, the graft is only partially immersed into the host *Hoxa13* domain of expression (G-O) but that by 48 h after grafting the entire graft is embedded in the host *Hoxa13* domain (P-R). Note also that the graft does not interfere with the dynamics of the host *Hoxa13* expression. The red asterisks mark the proximal limit of the graft. At least three examples for each experimental condition were analysed. Scale bars: 175 μm.

prospective zeugopod where they are initially placed may reflect different cell affinities between HH20 and later progenitor cells. It is known that cells from different stages and proximo-distal levels of the limb sort out, both *in vivo* and in culture, and this provides a read-out of positional values (Ide et al., 1994; Saiz-Lopez et al., 2015; Wada, 2011; Wada and Ide, 1994). It is also known that the product of the *Hoxa13* gene is one of the key determinants of this process (Stadler et al., 2001; Yajima et al., 2002). Therefore, the expression of *Hoxa13* could provide a segment-specific positional value to autopod cells that ensures that they contribute to the appropriate positional level when grafted to an earlier environment. A prediction of this is that the sorting out of *Hoxa13*-expressing and *Hoxa13*-non-expressing distal progenitor cells should be greater than between *Hoxa13*-expressing early and late autopod progenitors.

We tested this prediction using grafts made of a mixture of cells of different stages (Saiz-Lopez et al., 2015). Briefly, the distal 150 μm band of limb progenitors was dissected from GFP-expressing and wild-type wing buds, the cells dissociated, randomly mixed and reaggregated into a pellet from which 150 μm blocks were cut and

grafted under the AER of host HH20 buds (Fig. 3A,H). First, as a control, we used grafts made with labelled and unlabelled cells of the same stage as the host (Fig. 3A-G). In these control grafts, sorting out was not observed. Consecutive frontal sections hybridized for *Hoxa13* and *Gfp*, respectively, showed a random distribution of labelled cells within the graft in which *Hoxa13* had yet to be activated. Note that *Hoxa13* expression had initiated in posterior host tissue but not yet spread all along the anterior-posterior axis (Fig. 3B-D). However, a dramatic sorting out was observed within grafts made from random mixtures of HH20 (GFP labelled non-expressing *Hoxa13*) and HH24 (wild-type expressing *Hoxa13*) distal cells (Fig. 3H-N). By 24 h after grafting, *Hoxa13* expression could be detected throughout the graft, which mostly consisted of HH24 cells (7:1 proportion; Fig. 3I-K). Strikingly, the *Gfp*-expressing HH20 cells in such grafts were found exclusively around the periphery associating with host cells of the same age that were only just initiating *Hoxa13* expression (Fig. 3L-N). This finding reveals that *Hoxa13*-expressing and *Hoxa13*-non-expressing cells rapidly sort out *in vivo* and can explain why grafts of autopod progenitor cells made to an earlier environment become entrained into the distal part of the wing bud (Fig. 1).

The fact that *Hoxa13*-expressing HH24 and HH27 autopod progenitor cells show a similar developmental potential when grafted into the *Hoxa13*-non-expressing environment of HH20 zeugopod progenitor cells, could suggest that cell sorting is greater in cells from different presumptive segments, compared with cells from within the same segment. We tested this hypothesis using micromass cultures that were prepared with dissociated wild-type HH27 distal cells mixed with HH20 or HH24 GFP-expressing

distal cells. Previously, it has been shown that cells from different PD regions of chick wing buds sort out (Ide et al., 1994; Wada, 2011; Wada and Ide, 1994). As expected, labelled HH27 cells failed to segregate from wild-type HH27 cells whereas labelled HH20 cells strongly sorted out from them (Wada and Ide, 1994; Fig. 4A,B,E,F). Interestingly, sorting out between HH24 and HH27 cells was much attenuated (Fig. 4C,D) compared with HH20 and HH27 cells (Fig. 4E,F; Ide et al., 1998; Wada, 2011; Wada and Ide, 1994). For quantification, we used granulometry, which provides the size distribution of the distinct aggregates or 'granules' in the micromass cultures (see Materials and Methods). The results showed that the majority of the area occupied by labelled cells corresponded to single cells (71%; minor radius less than 4 μm) in HH27/HH27 mixtures while it corresponded to large aggregates (58%; minor radius larger than 12 μm) in HH27/HH20 micromasses. In micromasses made with mixtures of HH24/HH27 cells, 34% of the labelled area was occupied by single cells and 42% by small aggregates (minor radius between 4 and 8 μm). These results are consistent with cell surface properties being more similar within than between segments, and supports Hoxa13 as a major determinant of autopod cell-cell adhesion properties, as previously reported (Stadler et al., 2001; Yokouchi et al., 1995).

HH20 wings with HH27 grafts have a normal AER

Although HH24 and HH27 cells display identical positional values when grafted to HH20 wing buds, abnormal morphogenesis only occurs with the later HH27 grafts. To understand the reason for this difference, and the cause of the malformation, we considered whether the later grafts failed to maintain the AER since a localised defect in this structure is predicted to cause the observed phenotype.

During normal chick wing development, the distal mesenchyme maintains the AER until around HH29 at which time it regresses, and we have shown that this AER maintenance capacity is an intrinsic property of the distal mesenchyme (Saiz-Lopez et al., 2015; Scherz et al., 2004; Verheyden and Sun, 2008). To determine if grafts of HH27 distal mesenchyme lose the ability to maintain the AER as they age, and then if this would reciprocally fail to sustain development of the underlying mesenchyme, we grafted HH27 distal progenitors to HH20 buds and examined *Fgf8* expression in the AER over the graft (Fig. 5A-C). The AER can be seen either in frontal (flat) sections (Fig. 5A-C,G-I) or in longitudinal sections (Fig. 5D-F). Owing to the linear structure of the AER, usually only a portion of it is seen in frontal sections and therefore we selected the section in which the AER over the grafted tissue was present. We found a high level of *Fgf8* expression (similar to contralateral limb buds) in the AER overlying the donor tissue 24 h after grafting HH27 distal tips to HH20 hosts (Fig. 5A, arrow) when the stage of the graft if left *in situ* would have been HH29 (Fig. 5C). As expected, the AER is normally maintained over HH24 single (not shown) and serial grafts performed 24 h apart (Fig. 5D-F), which do not cause any malformation. To ensure that the donor tissue has progressed well beyond the age that it would normally support the AER, we performed serial grafts starting with HH27 distal progenitors and re-grafting after 48 h (Fig. 5G-I). In these experiments, expression of *Fgf8* in the AER over the graft was similar to the expression in the rest of the host AER even when analysed 48 h after the final graft (Fig. 5G). In addition, the stage of the grafted tissue if left in place would have been HH36 (Fig. 5I), clearly surpassing the stage when it would normally be able to maintain the AER.
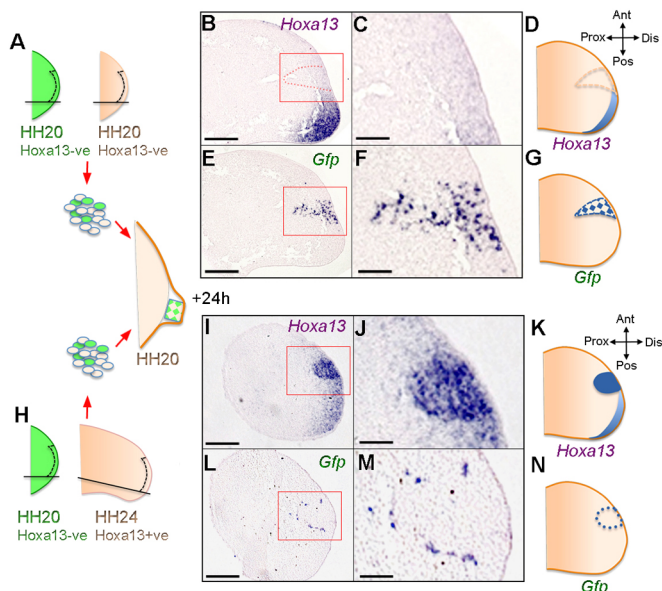
Fig. 3. Sorting out of *Hoxa13*-expressing and *Hoxa13*-non-expressing distal progenitor cells *in vivo*. (A-G) HH20 GFP-expressing and wild-type progenitor cells (A) randomly distribute in reaggregated grafts after 24 h as indicated by the expression of *Gfp* (E,F) as *Hoxa13* (B,C) has not been activated yet. (H-N) GFP-expressing HH20 and wild-type HH24 progenitor cells (H) sort out in reaggregated grafts within 24 h with the labelled cells preferentially located in the periphery of the graft in contact with the age-matched host cells, as indicated by the expression of *Hoxa13* (I,J) and *Gfp* (L,M). The distribution of cells in the re-aggregated grafts according to the expression patterns is schematically represented in D,G,K,N. Hoxa13-ve: Hoxa13 negative; Hoxa13+ve: Hoxa13 positive. Scale bars: 250 μm (B,E,I,L) and 100 μm (C,F,J,M).
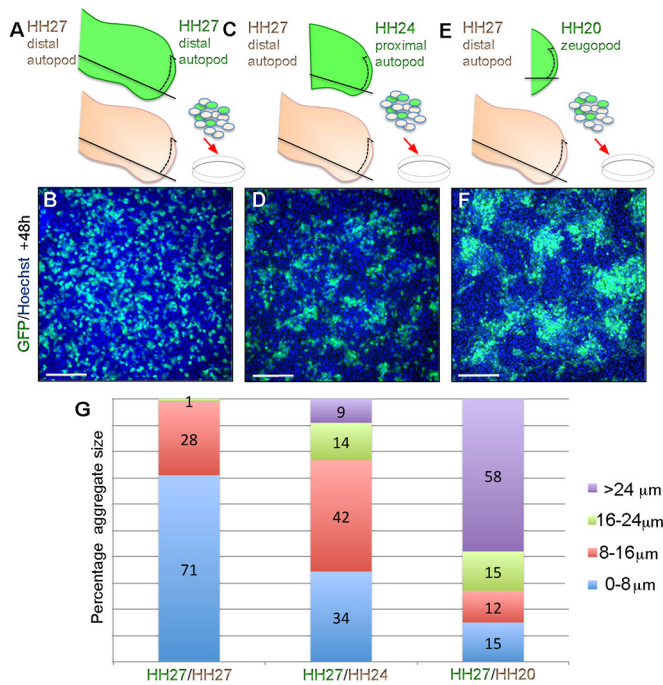
Fig. 4. Reduced sorting out of different stage *Hoxa13*-expressing cells *in vitro*. Mixtures of HH27 GFP-expressing and wild-type cells do not segregate in micromass cultures (A,B). Mixtures of GFP-expressing HH24 and wild-type HH27 distribute much more evenly (C,D) than mixtures of GFP-expressing HH20 and wild-type HH27 cells which readily sort out (E,F). Three examples for each experimental condition were analysed. (G) Granulometry graph showing the proportion of the total area occupied by different size aggregates, in each type of mixed micromass culture. The size of the minor diameter of the aggregate is indicated on the right. Scale bars: 200 μm.

These results clearly show that the malformations found in HH20 wings with HH27 grafts are not caused by an AER defect.

The cell cycle program of HH24 but not HH27 distal progenitor cells can be reset in an early environment

Since defective morphogenesis of HH20 wings with HH27 grafts is not a consequence of a failure in AER maintenance, we tested whether it could be a consequence of the decline in the cell cycle rate that occurs over normal development (Saiz-Lopez et al., 2015). To determine this, we performed flow cytometric analyses in HH27 (Fig. 6A) and single and serial grafts of HH24 distal progenitor cells placed under the AER of HH20 host buds (Fig. 6B,C). Interestingly, single grafts of HH27 distal mesenchyme cells grafted to HH20 buds had a reduced proliferative potential typical of their age (Fig. 6A). After 24 h, the proportion of G1-phase cells in the donor tissue was 81.1% compared with 59.3% in the equivalent region of HH24 distal mesenchyme in the contralateral wing (Fig. 6A). Thus, by this time, the donor tissue had a similar proportion (81.7%) of G1-phase cells as it would have had if allowed to develop *in situ* until HH29 (Saiz-Lopez et al., 2015). The retarded growth of the graft relative to host tissue could provide a reason for the defective morphogenesis in HH20 wings with HH27 grafts. If this is the case, the HH24 grafts, which do not cause malformations, should adapt their cell cycle program to that of the host. In fact, 24 h after grafting, the cell cycle profiles of HH24 single (Fig. 6B) and serial (two sequential grafts 24 h apart; Fig. 6C) grafted cells were very similar (G1 cells, 58.2% and 60.5%, respectively) to those found in the equivalent region of tissue in the contralateral (left-wing) limb buds of the same embryos (57.6% and 58%, respectively, Fig. 6B,C). It
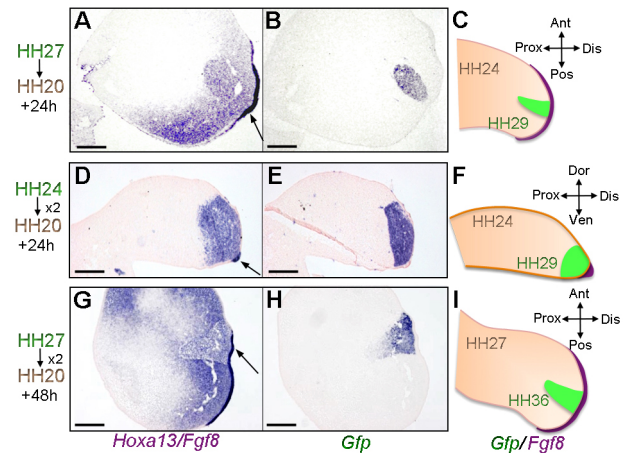

Fig. 5. Normal *Fgf8* expression in the AER over old grafts. Strong expression of *Fgf8* is observed in the AER over the graft of GFP-expressing HH27 to HH20 host wing buds 24 h after grafting (A-C). *Fgf8* expression is also normal over grafts of GFP-expressing HH24 serially transferred two times to HH20 host wing buds (D-F). The expression of *Fgf8* is also normal over serial HH27 grafts to HH20 host 48 h after grafting (G-I) even if the serial grafting is spaced by 48 h. (A,D,G) *Fgf8* is also hybridized with *Hoxa13*. *Fgf8* expression is shown in frontal (A,G) and longitudinal (D) sections also hybridized for *Hoxa13*. Note area of grafted tissue shown by *Gfp* expression (B,E,H) in consecutive sections to those hybridized for *Fgf8* and *Hoxa13* (A,D,G). On the right, the schematics for each experiment are shown in which the final age of the host and grafted tissue is indicated with the corresponding colour as well as the limb axes (C,F,I). Frontal sections are shown except for D-F, which are longitudinal sections. At least three examples for each experimental condition were analysed. Scale bars: 150 μm.

should be noted that G1-phase proportions differ by less than 2% in left and right buds of the same embryos and also those with homochronic grafts (see Saiz-Lopez et al., 2015). By this time, the donor tissue if left *in situ* would have developed until HH27 (Fig. 6B) and HH29 (Fig. 6C) and the proportion of G1-phase cells in distal mesenchyme at these stages are expected to be 64.5% and 81.7%, respectively (Saiz-Lopez et al., 2015). Thus, this result clearly shows that the cell cycle program of HH24 wing bud distal mesenchyme can be repeatedly reset in an HH20 environment.

Taken together, our results show that HH27 distal progenitor cells are refractory to signals from earlier distal environments that can reset the proliferation rate of HH24 progenitors. This is similar to what we found previously with the cells of the polarizing region (Chinnaiya et al., 2014). Thus, it is the developmental stage of the distal progenitors rather than the length of time for which they developed, that limits their ability to reset their cell cycle program in an early environment. It is very likely that the discrepancy in proliferation rates between host and donor tissue is the cause of the defective morphogenesis. We also investigated additional reasons for the defective morphogenesis in HH20 wings with HH27 grafts by inspecting for abnormal apoptosis by TUNEL (Fig. 6D-G). A sequential analysis of experimental wings with HH24 (used for comparison) and HH27 grafts failed to detect any abnormal apoptosis that could explain the truncation phenotype observed with HH27 grafts (Fig. 6F,G).

DISCUSSION

The recent observation that the distal structures of the limb are specified by an intrinsic timing mechanism has opened up new questions that we have addressed in this paper. Does this intrinsic timing mechanism ensure that the proximal to distal sequence of patterning events only occurs once, and if so, what are the
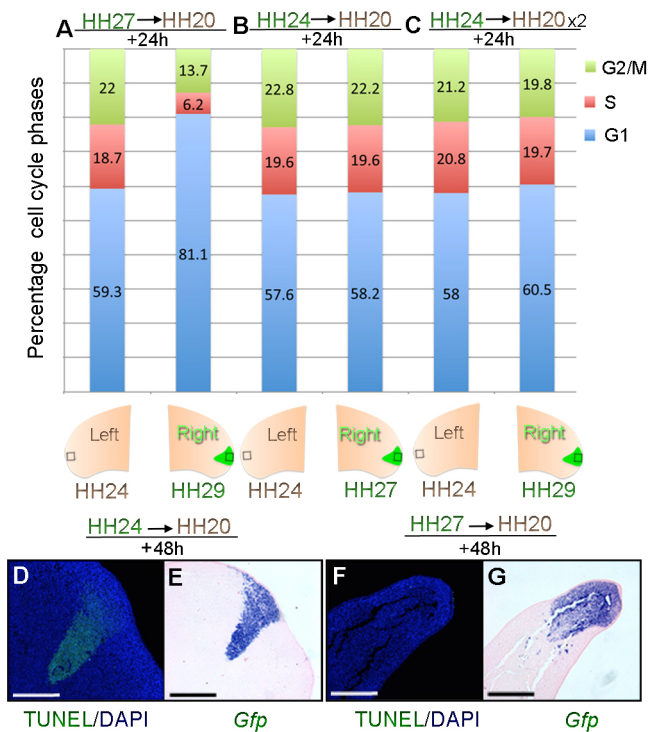
Fig. 6. Cell cycle parameters can be reset at HH24 but not at HH27. Distal HH27 cells maintain their cell cycle parameters even in a host earlier environment (A) while HH24 distal cells reset their cell cycle parameters to that of host equivalent cells within 24 h after grafting (B) and this resetting is maintained in serial grafts (C). Note that in A, there is a significant difference in G1-phase numbers between left and right wing buds (Pearson's χ^2 test, $P<0.05$) consistent with cell cycle parameters being maintained in donor tissue, and in B,C, there is a significant difference in G1-phase numbers between host values and expected values (Saiz-Lopez et al., 2015) for the stage of the donor tissue (Pearson's χ^2 test, $P<0.05$) consistent with cell cycle parameters of the graft being reset close to host levels. Note in all cases, 10-12 blocks of tissue were pooled from replicate experiments and run once. There is no abnormal cell death in heterochronic distal grafts (D-G). The TUNEL assay fails to detect abnormal cell death at any stage analysed during the development of the grafted limbs. One example for a HH24 to HH20 graft (D,E, frontal sections) and another for a HH27 to HH20 graft (F,G, longitudinal sections) are shown. In each case, the graft is detected in consecutive sections hybridized for Gfp (E,G). Note that the graft in D still maintains weak Gfp expression. Scale bars: 200 µm (D,F) and 275 µm (E,G).

mechanisms involved? We have discovered that expression of *Hoxa13*, the best marker of the autopod, is stable and irreversible, while other intrinsically timed processes, such as the rate of proliferation, show more plasticity. When transferred into an earlier environment, later progenitor cells can use their intrinsically determined *Hoxa13* status and segment-specific cell adhesive properties to allocate themselves into the correct segment. Early autopod progenitors, fated for the wrist, can adjust their proliferation rate and this ensures normal morphogenesis, while late autopod progenitors, fated to the phalanges, lose their proliferative plasticity and this perturbs host morphogenesis.

Positional values of the autopod are irreversibly determined as a segment-specific property

The heterochronic grafting experiments we describe here show that the positional values of HH24 (proximal autopod) and HH27 (distal autopod) progenitor cells are not reset to the host HH20 positional value. However, based on their normal fate, it was expected that these two types of grafts would have a different positional value and

therefore that the later grafts would contribute to more-distal structures. While it is possible that the earlier environment is capable of partially resetting HH27 cells, but not the relatively younger HH24 cells, a more reasonable interpretation of our results is that the positional value of all autopod progenitor cells, from the wrist to the distal phalanx of the digits, is more or less equivalent (and includes the whole autopod).

Experimental evidence both *in vivo* and *in vitro* indicates that the translation of proximo-distal positional values into an anatomically distinct morphology is mediated by position-specific cell-cell affinities (Ide et al., 1994; Wada, 2011). These position-specific cell surface properties are considered to be progressively acquired under the AER as a continuous cellular gradient along the PD axis (Barna and Niswander, 2007; Nardi and Stocum, 1984; Tamura et al., 1997). Their presence is revealed by the sorting out that occurs when progenitor cells of different proximo-distal levels or ages are confronted (Friedlander et al., 1989; Steinberg and Takeichi, 1994). It is also known that cell-cell adhesion properties are influenced by 5′ Hox transcription factors, in particular, Hoxa13 (Ide et al., 1998; Cobb and Duboule, 2005; Stadler et al., 2001; Wada et al., 2003; Yokouchi et al., 1995). The fact that *Hoxa13* expression is robustly maintained in the grafts strongly indicates that cell surface properties are also maintained, and therefore, we propose that the stable expression of *Hoxa13* is responsible for graft entrainment into the host *Hoxa13* domain.

Our data also indicate that, at least for the autopod, cell-cell affinities are segment specific. However, despite the common expression of *Hoxa13*, a reduced amount of sorting out still remains between HH24 and HH27 distal progenitors, suggesting that factors additional to Hoxa13 also control cell surface properties. However, it should be noted that a possible differential level of *Hoxa13* expression over development, and hence of downstream effectors of cell adhesion, could also contribute to the remaining sorting out between HH24 and HH27 progenitor cells.

If an important role exists for Hoxa13 in the acquisition of positional values, it is therefore surprising that the loss of *Hoxa13* function in the mouse limb results in normal proximo-distal patterning (Fromental-Ramain et al., 1996; Stadler et al., 2001). $Hoxa13^{-/-}$ mutants exhibit oligodactyly as the entire first digit is absent and autopod progenitors lacking *Hoxa13* show an impaired capacity to form cartilage condensations *in vitro* (Stadler et al., 2001). However, it should be noted that *Hoxd13* can substitute for *Hoxa13* and, in fact, the condensations of digits 2 to 5 do not form in compound $Hoxa13^{-/-};Hoxd13^{-/-}$ mutants (Fromental-Ramain et al., 1996).

Embryonic proliferation plasticity ensures normal morphology

Since cells of HH24 and of HH27 grafts have equivalent positional values in an earlier HH20 environment and display similar *Hoxa13* expression dynamics, it was an unexpected finding that morphogenesis of the HH20 host is severely altered only with HH27 grafts. Serial grafts of HH24 cells, in which the final age of the graft is much older than HH27, do not disrupt morphogenesis, thus indicating that it is the developmental stage of the tissue and not the length of time for which it has developed that disrupts development of the host. Following the various single and serial grafts of HH24 cells and single and serial grafts of HH27 cells we made to HH20 buds, the host AER was maintained and no abnormal cell death was observed, therefore excluding these two factors as a cause of the growth defect. It should be noted that our experiments do not rule out the possibility that the old distal progenitors do

indeed lose their ability to maintain the AER, because it is possible that this function is replaced by the surrounding host tissue, but they do rule out an AER defect as a cause of the malformation.

Remarkably, distinct differences in proliferation were observed, depending on the type of graft. In the case of HH24 grafts, the cell cycle profile was reset to match that of the host environment and this permitted normal morphogenesis. However, in the case of HH27 grafts, the cell cycle profile was not reset to host values and thus interfered with normal morphogenesis. Therefore, this result indicates that early autopod progenitors are still capable of responding to host signals, but that they become refractory before reaching HH27. The ability of cells to reset their cell cycle parameters until relatively late stages could confer robustness to embryonic patterning. Therefore, although disparities in positional values can be tolerated because cells actively sort out, disparities in proliferation rate can only be tolerated if cells can adapt their rate to that of the environment. Our results also show that the inability of a group of cells to adapt to the proliferation rate of the surrounding tissue may disrupt normal morphogenesis in a non cell-autonomous manner.

Implications for regeneration
On a more general note, positional information has been extensively studied in amphibian limb regeneration and is considered to be of a continuously graded nature along the proximo-distal axis. Indeed, recent studies using transgenic axolotl lines have shown that the nature of positional information is rather cell autonomous, mainly restricted to the cartilage/fibroblast lineage and dependent on the cellular memory of the tissue of embryonic origin (Maden et al., 2015). During axolotl limb regeneration, cells are able to re-express the appropriate position-specific Hoxa gene at the amputation plane and then transit progressively through sequential distal fates as missing tissues are restored (Roensch et al., 2013). Most interestingly, heterochronic transplantation of blastema cells also showed the correlation between *Hoxa13* expression and commitment to hand identity similar to what we have observed in this study (Roensch et al., 2013).

An equivalent cellular memory is observed in mammals, as limb skeletal elements retain expression of segment-specific markers up to late differentiation stages, and also the origin and molecular status of skeletal progenitor cells influences the process of adult bone regeneration (Leucht et al., 2008; Roselló-Díez et al., 2011). Therefore, based on our data presented here, we speculate that cells acquire positional values during the patterning phase of embryogenesis and use this information to direct the formation of the appropriate missing structures during potential regeneration events. However, during regeneration the progressive expression of 5′ Hoxa genes must be recoupled to stage-specific proliferation to achieve the correct morphology. Therefore, the inability to reset the proliferation rate beyond embryogenesis to that typical of the corresponding patterning phase could contribute to regenerative failure in most limbs. Interestingly, important progress towards the identification of factors that induce the initial cell cycle response during axolotl appendage regeneration has been recently reported (Sugiura et al., 2016). It is of major importance to determine what limits proliferation plasticity in most vertebrate limbs.

MATERIALS AND METHODS
Tissue grafting
Tissue grafts were performed as described in Saiz-Lopez et al. (2015). Briefly, the distal 150 µm tip of GFP-expressing donor wing buds

(excluding the posterior border containing the polarizing region) was dissected, the overlying ectoderm removed by mild trypsin incubation and the stripe then cut into cuboidal pieces. For serial grafting, 24 h or 48 h after the first graft was performed, the distal 150 µm tip of the GFP-expressing tissue was dissected, the ectoderm was peeled off and cut into cuboidal pieces that were used for a second graft. For sorting out experiments, the distal stripes of GFP-expressing and wild-type wing buds were dissociated to single cell level, randomly mixed and reaggregated by mild centrifugation to obtain a pellet from which 150 µm^2 cuboidal pieces were cut. To better distinguish the labelled cells, a proportion of 1:7 with wild-type cells was used. Each block was placed under the AER of a wild-type host embryo and the development of the graft monitored under UVA light. In some cases, the blocks were grafted in a proximal location, corresponding to the stylopod or zeugopod, as desired. The skeletal pattern was visualized after Alizarin Red-Alcian Blue staining. All experiments were repeated at least three times and at least three embryos for each condition were analysed.

In situ hybridization and cell death assays
In situ hybridization was performed on paraffin sections of 4% paraformaldehyde fixed specimens as previously described (Saiz-Lopez et al., 2015) using digoxigenin-labelled riboprobes directed against *Sox9*, *Gfp*, (Fisher et al., 2011), *Fgf8* (Crossley et al., 1996) and *Hoxa13* (Nelson et al., 1996). Detection of cell death was also performed in paraffin sections using terminal deoxynucleotidyl transferase mediated dUTP nick-end labelling (TUNEL) with the Apoptag Fluorescein Direct In Situ Apoptosis Detection Kit (Intergen) according to the manufacturer's instructions. At least three examples for each experimental condition were analysed.

Micromass culture
For micromass cultures, distal stripes of GFP-expressing and normal wing buds were obtained and disaggregated to single cells by gentle pipetting after removal of the ectoderm. Then the cells were counted and mixtures of the labelled and non-labelled cells at a 1:3 ratio were performed. The cells were then resuspended and plated in 10 µl drops at a density of $2×10^6$ per ml. After 1 h, DMEM/F12 Glutamax medium containing 10% fetal calf serum and 1% penicillin-streptomycin was added. The cultures were sequentially fixed and the distribution of GFP-expressing cells examined by fluorescent microscopy. At least three examples for each experimental condition were analysed.

Flow cytometry
Normal and GFP-expressing distal tip tissue was dissected in ice-cold PBS under a Leica MZ16F UV microscope using a fine surgical knife, pooled from replicate experiments (between 10 and 12), and digested into single cell suspensions with trypsin (0.5%, Gibco) for 30 min at room temperature. Cells were washed twice in PBS, fixed in 70% ethanol overnight, washed again twice in PBS and resuspended in PBS containing 0.1% Triton X-100, 50 µg ml^{-1} propidium iodide and 50 µg ml^{-1} of RNase A (Sigma). Dissociated cells were left at room temperature for 20 min, aggregated cells were removed by filtration and then analysed for DNA content with a FACSCalibur flow cytometer and FlowJo software (Treestar). Based on ploidy values, cells were assigned in G1, S or G2/M phases and this was expressed as a percentage of the total cell number (8000-10,000). Statistical significance was determined by Pearson's χ^2 tests to obtain two-tailed P-values ($P<0.05$ was considered to represent a significant difference).

Granulometry
For quantification of the size of the cell aggregates in the micromass cultures, we used Granulometry, which provides the size distribution of the distinct aggregates or 'granules'. For this, the micromasses were photographed and the images thresholded to create a binary mask of the GFP-positive aggregates for automated morphological analysis (Fiji). This mask was sequentially subject to erosion, removing pixels on the border of the aggregate, and then to dilation, adding pixels on the border of the aggregate, for a number of times (opening cycles). If erosion is smaller than the minor diameter of a cluster, it approximately recovers its initial size during dilation. However, when the erosion length is bigger than the diameter of a cluster, it is

deleted during erosion and not recovered by dilation. For each cycle, the sum of all GFP-positive areas is computed and plotted.

Supplementary information
Supplementary information available online at
http://dev.biologists.org/lookup/doi/10.1242/dev.137661.supplemental

References
Barna, M. and Niswander, L. (2007). Visualization of cartilage formation: insight into cellular properties of skeletal progenitors and chondrodysplasia syndromes. *Dev. Cell* 12, 931-941.

Cobb, J. and Duboule, D. (2005). Comparative analysis of genes downstream of the Hoxd cluster in developing digits and external genitalia. *Development* 132, 3055-3067.

Cooper, K. L., Hu, J. K.-H., ten Berge, D., Fernandez-Teran, M., Ros, M. A. and Tabin, C. J. (2011). Initiation of proximal-distal patterning in the vertebrate limb by signals and growth. *Science* 332, 1083-1086.

Crossley, P. H., Minowada, G., MacArthur, C. A. and Martin, G. R. (1996). Roles for FGF8 in the induction, initiation, and maintenance of chick limb development. *Cell* 84, 127-136.

Chinnaiya, K., Tickle, C. and Towers, M. (2014). Sonic hedgehog-expressing cells in the developing limb measure time by an intrinsic cell cycle clock. *Nat. Commun.* 5, 4230.

Delgado, I. and Torres, M. (2016). Gradients, waves and timers, an overview of limb patterning models. *Semin. Cell Dev. Biol.* 49, 109-115.

Dudley, A. T., Ros, M. A. and Tabin, C. J. (2002). A re-examination of proximodistal patterning during vertebrate limb development. *Nature* 418, 539-544.

Fernandez-Teran, M. and Ros, M. A. (2008). The apical ectodermal ridge: morphological aspects and signaling pathways. *Int. J. Dev. Biol.* 52, 857-871.

Fisher, M., Downie, H., Welten, M. C. M., Delgado, I., Bain, A., Planzer, T., Sherman, A., Sang, H. and Tickle, C. (2011). Comparative analysis of 3D expression patterns of transcription factor genes and digit fate maps in the developing chick wing. *PLoS ONE* 6, e18661.

Friedlander, D. R., Mege, R. M., Cunningham, B. A. and Edelman, G. M. (1989). Cell sorting-out is modulated by both the specificity and amount of different cell adhesion molecules (CAMs) expressed on cell surfaces. *Proc. Natl. Acad. Sci. USA* 86, 7043-7047.

Fromental-Ramain, C., Warot, X., Messadecq, N., LeMeur, M., Dollé, P. and Chambon, P. (1996). Hoxa-13 and Hoxd-13 play a crucial role in the patterning of the limb autopod. *Development* 122, 2997-3011.

Hamburger, V. and Hamilton, H. L. (1951). A series of normal stages in the development of the chick embryo. *J. Morphol.* 88, 49-92.

Ide, H., Wada, N. and Uchiyama, K. (1994). Sorting out of cells from different parts and stages of the chick limb bud. *Dev. Biol.* 162, 71-76.

Ide, H., Yokoyama, H., Endo, T., Omi, M., Tamura, K. and Wada, N. (1998). Pattern formation in dissociated limb bud mesenchyme in vitro and in vivo. *Wound Repair Regen.* 6, 398-402.

Leucht, P., Kim, J.-B., Amasha, R., James, A. W., Girod, S. and Helms, J. A. (2008). Embryonic origin and Hox status determine progenitor cell fate during adult bone regeneration. *Development* 135, 2845-2854.

Maden, M., Avila, D., Roy, M. and Seifert, A. W. (2015). Tissue specific reactions to positional discontinuities in the regenerating axolotl limb. *Regeneration* 2, 137-147.

McGrew, M. J., Sherman, A., Ellard, F. M., Lillico, S. G., Gilhooley, H. J., Kingsman, A. J., Mitrophanous, K. A. and Sang, H. (2004). Efficient production of germline transgenic chickens using lentiviral vectors. *EMBO Rep.* 5, 728-733.

Nardi, J. B. and Stocum, D. L. (1984). Surface properties of regenerating limb cells: Evidence for gradation along the proximodistal axis. *Differentiation* 25, 27-31.

Nelson, C. E., Morgan, B. A., Burke, A. C., Laufer, E., DiMambro, E., Murtaugh, L. C., Gonzales, E., Tessarollo, L., Parada, L. F. and Tabin, C. (1996). Analysis of Hox gene expression in the chick limb bud. *Development* 122, 1449-1466.

Pascoal, S., Carvalho, C. R., Rodriguez-León, J., Delfini, M.-C., Duprez, D., Thorsteinsdóttir, S. and Palmeirim, I. (2007). A molecular clock operates during chick autopod proximal-distal outgrowth. *J. Mol. Biol.* 368, 303-309.

Roensch, K., Tazaki, A., Chara, O. and Tanaka, E. M. (2013). Progressive specification rather than intercalation of segments during limb regeneration. *Science* 342, 1375-1379.

Roselló-Díez, A., Ros, M. A. and Torres, M. (2011). Diffusible signals, not autonomous mechanisms, determine the main proximodistal limb subdivision. *Science* 332, 1086-1088.

Roselló-Díez, A., Arques, C. G., Delgado, I., Giovinazzo, G. and Torres, M. (2014). Diffusible signals and epigenetic timing cooperate in late proximo-distal limb patterning. *Development* 141, 1534-1543.

Saiz-Lopez, P., Chinnaiya, K., Campa, V. M., Delgado, I., Ros, M. A. and Towers, M. (2015). An intrinsic timer specifies distal structures of the vertebrate limb. *Nat. Commun.* 6, 8108.

Scherz, P. J., Harfe, B. D., McMahon, A. P. and Tabin, C. J. (2004). The limb bud Shh-Fgf feedback loop is terminated by expansion of former ZPA cells. *Science* 305, 396-399.

Scotti, M., Kherdjemil, Y., Roux, M. and Kmita, M. (2015). A Hoxa13:Cre mouse strain for conditional gene manipulation in developing limb, hindgut, and urogenital system. *Genesis* 53, 366-376.

Stadler, H. S., Higgins, K. M. and Capecchi, M. R. (2001). Loss of Eph-receptor expression correlates with loss of cell adhesion and chondrogenic capacity in Hoxa13 mutant limbs. *Development* 128, 4177-4188.

Steinberg, M. S. and Takeichi, M. (1994). Experimental specification of cell sorting, tissue spreading, and specific spatial patterning by quantitative differences in cadherin expression. *Proc. Natl. Acad. Sci. USA* 91, 206-209.

Sugiura, T., Wang, H., Barsacchi, R., Simon, A. and Tanaka, E. M. (2016). MARCKS-like protein is an initiating molecule in axolotl appendage regeneration. *Nature* 531, 237-240.

Summerbell, D. (1974). Interaction between the proximo-distal and antero-posterior co-ordinates of positional value during the specification of positional information in the early development of the chick limb-bud. *J. Embryol. Exp. Morphol.* 32, 227-237.

Suzuki, T., Hasso, S. M. and Fallon, J. F. (2008). Unique SMAD1/5/8 activity at the phalanx-forming region determines digit identity. *Proc. Natl. Acad. Sci. USA* 105, 4185-4190.

Tabin, C. and Wolpert, L. (2007). Rethinking the proximodistal axis of the vertebrate limb in the molecular era. *Genes Dev.* 21, 1433-1442.

Tamura, K., Yokouchi, Y., Kuroiwa, A. and Ide, H. (1997). Retinoic acid changes the proximodistal developmental competence and affinity of distal cells in the developing chick limb bud. *Dev. Biol.* 188, 224-234.

Towers, M., Wolpert, L. and Tickle, C. (2012). Gradients of signalling in the developing limb. *Curr. Opin. Cell Biol.* 24, 181-187.

Vargesson, N., Kostakopoulou, K., Drossopoulou, G., Papageorgiou, S. and Tickle, C. (2001). Characterisation of hoxa gene expression in the chick limb bud in response to FGF. *Dev. Dyn.* 220, 87-90.

Verheyden, J. M. and Sun, X. (2008). An Fgf/Gremlin inhibitory feedback loop triggers termination of limb bud outgrowth. *Nature* 454, 638-641.

Wada, N. (2011). Spatiotemporal changes in cell adhesiveness during vertebrate limb morphogenesis. *Dev. Dyn.* 240, 969-978.

Wada, N. and Ide, H. (1994). Sorting out of limb bud cells in monolayer culture. *Int. J. Dev. Biol.* 38, 351-356.

Wada, N., Tanaka, H., Ide, H. and Nohno, T. (2003). Ephrin-A2 regulates position-specific cell affinity and is involved in cartilage morphogenesis in the chick limb bud. *Dev. Biol.* 264, 550-563.

Yajima, H., Hara, K., Ide, H. and Tamura, K. (2002). Cell adhesiveness and affinity for limb pattern formation. *Int. J. Dev. Biol.* 46, 897-904.

Yokouchi, Y., Nakazato, S., Yamamoto, M., Goto, Y., Kameda, T., Iba, H. and Kuroiwa, A. (1995). Misexpression of Hoxa-13 induces cartilage homeotic transformation and changes cell adhesiveness in chick limb buds. *Genes Dev.* 9, 2509-2522.